JOURNAL OF MATERIALS SCIENCE **36** (2001) 1789–1799

Stress measurements on chrome-tanned leather

M. TUCKERMANN, M. MERTIG, W. POMPE
Institut für Werkstoffwissenschaft, Technische Universität Dresden, D-01062 Dresden, Germany
E-mail: mertig@tmfs.mpgfk.tu-dresden.de

G. REICH
Forschungsinstitut für Leder- und Kunstledertechnologie, D-09581 Freiberg, Germany

A sensitive method has been developed for the measurement of mechanical stresses in compliant planar samples originating from changes of their solvent content or temperature. The samples are mechanically conjoined with a silicon wafer. Thus, an alteration of the sample stress causes a spatial displacement of the wafer which is detected capacitively. The method is applied to the measurement of stresses in both acetone-dried and air-dried chrome-tanned leather which has been exposed to a stepwise modulation of ambient humidity. The stress development in the sample can be well characterized by a first-order exponential decay. The mean moisture content exhibits a similar time dependence. However, the relation between stress development and moisture content differs for swelling and shrinkage. This behavior is explained on the basis of a novel two-capillary model. Moreover, the response of the sample to the alteration of ambient humidity is found to be related to the structure of its collagen fiber network. The tight structure of air-dried leather with a poor isolation of fibrils yields much higher stresses than acetone-dried leather.

1. Introduction

The corium, the main layer of animal hides, is the raw material for leather manufacturing. It consists of a tight network of collagen fibers and fibrils, the water sorption of which, and therefore swelling and shrinkage of the network, strongly depend on temperature, humidity and pH. The process of drying is known to be the most important fabrication step in leather manufacturing since it determines already to a wide extent the resulting properties of the leather depending on the structural alignment of its fibers. The latter is influenced by capillary forces during water removal from the specimen. Therefore, different drying pathways can lead to variant leather quality. Because of the importance of the area yield for the leather industry, there is a great demand for fast and technically robust methods to characterize the drying behavior of differently treated leathers *in situ* during manufacturing.

Also in further processing the viscoelastic properties of leather are very important. One current example is the usage of leather for surface finishing of automotive dashboards. If unsuitable leather is used, dashboards can be deformed due to growing mechanical stresses under the influence of high temperature and low humidity. Also in shoe manufacturing the stress formation in leather during the lasting process (especially during "heat setting") is of great interest.

In this paper, a novel technique is described by which the stress development in leather can be recorded directly under changing environmental conditions. In distinction to previous methods, no static stress component is superimposed. Thus, small deformations can be detected with a higher accuracy than in common stress-strain investigations by tensile testing machines [1]. The characteristic differential strain in the studies discussed below is in the range of about 1×10^{-3} to 5×10^{-3}. This is about one order of magnitude smaller than achieved in the "low strain region" of common stress-strain investigations [2, 3]. Strain due to external forces is completely avoided by fixing the unstrained, planar material on a mechanically stiffer substrate which acts as flexible plate of a capacitor. Thus, shrinkage or expansion of the specimen under investigation, induced by environmental driving forces such as temperature or humidity, cause a spatial displacement of the substrate which can be detected capacitively with high resolution. This technique also allows a more precise evaluation of conformational changes of leather than corresponding stress-free strain measurements of unconstrained leather.

Besides methodical aspects, this paper mainly focuses on the investigation of the dependence of the mechanical stress, σ, on the moisture content, c, of leather. Both entities are controlled dynamically by the relative humidity of the surrounding air at constant temperature.

2. Experimental and materials

2.1. Capacitive stress measurement transducer

The method for detection of stresses in plain leather sheets is based on the measurement of the deformation of a mechanically attached disk of known elastic

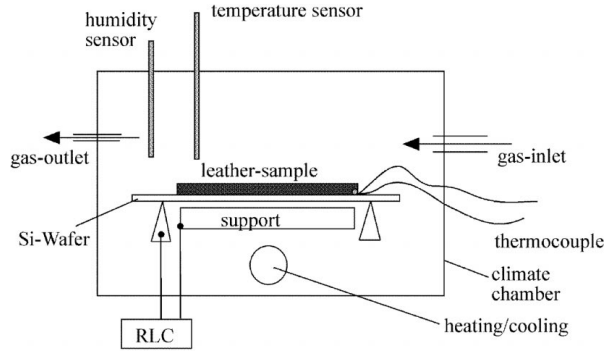

Figure 1 Schematic viegraph of the experimental set-up used for the stress measurements. The capacitive stress transducer is mounted in a climate chamber. Differential shrinkage or swelling of the leather sample, glued to a Si wafer, results in a slight bending of the wafer. This bending is measured by recording the capacity change between the Si wafer, which is metal-coated on the bottom side, and the metallic support with an AC capacitance bridge (RCL).

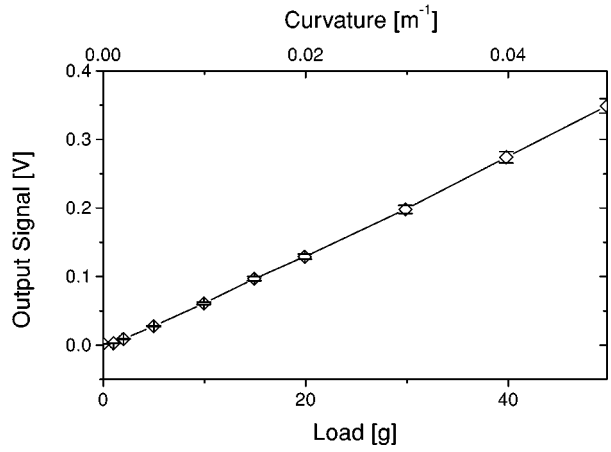

Figure 2 Calibration curve of the stress measuring device. External loads provoke different curvature of the Si wafer. These are observed by an optical displacement meter and correlated with the output voltage signal of the capacitive transducer device.

constants. Shrinkage or expansion of the leather are transferred into a smooth curvature of the disk caused by the stress in the substrate which is *a priori* not sensitive to anisotropic behavior. Thus, shrinkage or expansion of the fiber network can be quantified in terms of forces. In similar techniques the disk curvature is usually detected by a laser displacement meter [4] or optical interference techniques [5]. However, optical methods require a high reflectivity of the materials surfaces. To overcome this disadvantage, we measure the curvature of the disk by monitoring the capacity change between the metal coated bottom side of the disk and a fixed capacitor plate (see Fig. 1) following the technique developed by Willcock and Campell [6]. Previously, the capacitive transducer technique has been e.g. successfully applied to gas pressure gauges [7], and to stress measurement of both thin growing films [8] and drying ceramic precursors [9].

In order to employ substrate disks with reproducible mechanical properties, we have used Si wafers (*Wacker Siltronik, Freiberg, Germany*) with a thickness of 380 μm and a diameter of 3 Inch. In addition, the wafers have been electrochemically metallized from the bottom side with a gold layer of about 1 μm thickness. The capacitive change due to differences in the disk curvature were detected with a Wheatstone bridge, which was operated at 10 kHz. The system was calibrated by measuring the capacity changes for different loading of the pure Si-wafer. The corresponding voltage output signal of the Wheatstone bridge is given in Fig. 2. This signal turned out to depend nearly linearly on the applied load in the region investigated. Simultaneously, the corresponding disk curvatures were recorded with an optical topography scanner (*FLEXUS-2140, KLA-TENCOR, Canada*). The long-term stability of the built-up capacitive transducer is smaller than 2 mV measured over a period of 10 h. The temperature coefficient is 15 mV/K.

With this system, differences in the disk curvature down to 1.3×10^{-4} m^{-1} could be detected corresponding about to a wafer displacement of 0.1 μm and/or a stress of 0.5 Pa. However, the sensitivity can easily be improved by more than a factor of ten if necessary.

The capacity transducer device is placed in a climate chamber, in which the temperature and the relative humidity can be controlled (Fig. 1). The relative humidity is adjusted by mixing a dry and a wet gas stream. In this way, the relative humidity can be adjusted between 5% and 90% at a temperature of about 25°C, avoiding condensation of water or very high gas flow rates. Thus, gradients of both humidity and temperature are suppressed within the climate chamber. Typically, the characteristic relaxation time for switching from one to another humidity value is less than two minutes. Temperature and humidity of the air in the climate chamber are measured with a P570 sensor (*Dostmann Electronic GmbH, Wertheim, Germany*). The data acquisition of stress and climate values was usually done every 10 s to 60 s. The humidity coefficient of the pure wafer system is, as expected, extremely low. It corresponds to 0.2 mV per 1% relative humidity change. For the measurements presented, usually the following humidity-time regime was chosen: at the beginning of the experiment the relative humidity is set to a default value of 50% and kept there overnight to achieve equilibrium conditions; then, the humidity was cycled twice for one hour to 20%; thereafter, it was two times increased to 80% for one hour each cycle. The temperature is kept constant over the duration of whole experiment.

2.2. Investigated samples and preparation

All investigations were done with chrome-tanned bovine leather without any additional retannage, fatliquoring or finishing. The samples originate from the butt of the hide. After passing the beamhouse they were tanned with 1.3% Cr_2O_3 per pelt weight. Thereafter, one half of the samples were acetone dried, and the other half were air dried. The two drying procedures result in remarkable differences in the sample thickness of 2.4 mm and 1.0 mm, respectively. In addition, some of the acetone-dried samples were split into a grain layer, how the surface layer of leather is usually called, an upper corium layer and a lower corium layer. The apparent thickness of these layers was 0.7 mm, 1.1 mm and 0.9 mm, respectively.

The samples (grain side facing the wafer) were glued onto the uncoated side of the Si wafers with a two-component epoxy glue (*UHU plus schnellfest, UHU*

GmbH, Bühl, Germany) at a relative humidity of about 50%. The glue was applied on the Si wafer as an about 10 μm thick film by means of a slanting plate. The leather samples are fixed without applying lateral stresses.

2.3. Characterization of sample structure

2.3.1. SEM observation

Both, acetone- and air-dried leather samples, have been examined by low-voltage scanning electron microscopy (*GEMINI DSM-982, ZEISS, Oberkochen, Germany*) at 1 kV allowing fibrillar resolution of the leather microstructure. For these examinations the samples have been cross sectioned by a microtome (*HM340E, Microm Laborgeräte GmbH, Walldorf, Germany*) and afterwards coated with an about 30 nm thick sputtered Pt film.

2.3.2. Porosity and inner surface

Porosity has been estimated in two different ways: first, from density considerations, and alternatively, a 2D porosity has been derived from SEM image analysis, i.e., the area of pores has been analyzed in relation to the entire image area. The inner surface has been determined by the specific adsorption of nitrogen (BET) after Brunauer, Emmet and Teller [10] (*ASAP 2000, MICROMERITICS, Norcross, USA*), employing ≈ 2.5 g of leather, cut into pieces of 5 mm $\times$ 5 mm in size, for one measurement. The typical equilibration times are $>$11 h. The BET measurement yields a value in units of surface per weight, which is of course not directly related to the dimensionless volume porosity. However, this value takes the separation of structure elements in the range of a few nanometers more specifically into account.

2.3.3. Moisture-sorption characteristic

Moisture-sorption characteristics have been obtained via mass analysis of the samples by an analytical balance (*AT 200, Mettler, Greifensee, Switzerland*). For this, the gas mixing system from the stress-measurement device including the temperature/ humidity sensor has been adapted to the balance housing. All measurements were performed with samples mounted on Si wafers.

2.4. Data analysis

In general, forces and thermodynamical state variables characterizing the stress development in a planar sample depend on spatial position, (x, y, z), and time, t. In our particular case, the stress in the flat, cylindrical sample can be well described by an isotropic biaxial stress state because of the sample symmetry. Moreover, neglecting thickness variations of the stress field, we can average over the sample thickness, h. This leads to state variables depending only on time. According to [11], the mechanical stress in linear and isotropic materials under isothermal conditions, $\bar{\sigma}(t)$, can be described by

$$\bar{\sigma}(t) = \frac{E}{1-\nu} \cdot (\bar{\epsilon}(t) - \beta \Delta \bar{c}(t)), \qquad (1)$$

where E is the Young's modulus, ν is the Poisson's ratio, $\bar{\epsilon}(t)$ is the strain, $\bar{c}(t)$ is the moisture concentration and β is a constant factor. The overlined symbols denote thickness averages.

In our experiment, the average stress in the leather layer, $\bar{\sigma}_L^*$, has to be derived from the curvature of the conjoined system, κ. This can be obtained by taking into consideration that Equation 1 is valid for each individual layer:

$$\bar{\sigma}_L^*(t) = \frac{E_L}{1-\nu_L} \cdot (\bar{\epsilon}_L(t) - \beta \cdot \bar{c}(t)),$$

$$\bar{\sigma}_{Si}(t) = \frac{E_{Si}}{1-\nu_{Si}} \cdot \bar{\epsilon}_{Si}(t). \qquad (2)$$

Here, the indexes Si and L denote the wafer and the leather, respectively. Using Kirchhoff's theory for layered plates [12] with $\bar{\epsilon}_{Si} = \bar{\epsilon}_L$ and $\bar{\sigma}_{Si} \cdot h_{Si} + \bar{\sigma}_L^* \cdot h_L = 0$, $\bar{\sigma}_L^*$ can be calculated by:

$$\bar{\sigma}_L^*(t) = \frac{E_{Si} \cdot h_L}{6 \cdot (1-\nu_{Si}) \cdot \rho^2 \cdot (1+\rho)} \cdot (1 + e\rho^3) \cdot \kappa(t). \qquad (3)$$

Here, the dimensionless factors ρ and e are given by $\rho = \frac{h_L}{h_{Si}}$ and $e = \frac{E_L(1-\nu_{Si})}{E_{Si}(1-\nu_L)}$.

In Equation 3 all values are revealed except of e because E_L and ν_L are unknown. Therefore, it is not possible to calculate $\bar{\sigma}_L^*$ directly from Equation 3. Usually, at this point the Stoney's approximation ($\rho \ll 1$) is applied for thin films [13]. However, the layer thickness of the leather samples is large compared to the Si-wafer thickness. In our case, ρ ranges from 2 to 5. Therefore, we have evaluated the factor $(1+e \cdot \rho^3)$ of Equaton 3 taking into consideration that e for soft materials like leather ranges between 1×10^{-3} and 5×10^{-3}. In Fig. 3 the ratio $\frac{1}{(1+e \cdot \rho^3)}$ is plotted versus the leather sample thickness for different e. On the one hand, it can be seen that $e \times \rho^3$ is much smaller than 1 for $h_L < 1$ mm. In this case Equation 3 reduces to:

$$\bar{\sigma}_L(t) = \frac{E_{Si} \cdot h_L}{6 \cdot (1-\nu_{Si}) \cdot \rho^2 \cdot (1+\rho)} \cdot \kappa(t), \qquad (4)$$

so

$$\frac{\bar{\sigma}_L}{\bar{\sigma}_L^*} = \frac{1}{1 + e \cdot \rho^3}. \qquad (5)$$

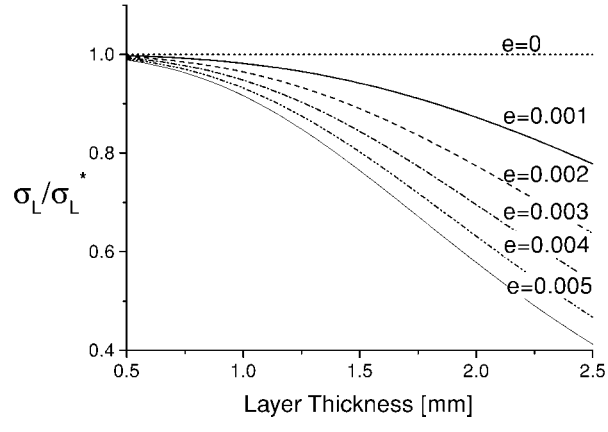

Figure 3 The dependence of the ratio $\frac{\bar{\sigma}_L}{\bar{\sigma}_L^*}$ on the leather sample thickness according to Equation 5 for different values of e.

Here, $\bar{\sigma}_L$ is the stress of the leather sample for $h_L \to 0$. On the other hand, Fig. 3 illustrates that it is possible to obtain an estimate for e by plotting the thickness dependence of $\frac{\bar{\sigma}_L}{\sigma_L^*}$ and fitting the results with Equation 5.

2.5. Description of the stress relaxation

Exchange and loading processes in finite volumes under stepwise-constant driving forces can be described by an exponential decay function $f(t) = f_0 + \sum_i A_i \cdot \exp(-\frac{(t-t_0)}{\tau_i})$ with a spectrum of relaxation times τ_i [14], which reduces in the case of only one dominating mechanism to:

$$f(t) = f_0 + A \cdot \exp\left(-\frac{(t-t_0)}{\tau}\right). \qquad (6)$$

In our case the dominating driving force for the stress development is the relative humidity since temperature is kept constant during the experiment. In accordance to this, we observed that the stepwise change of humidity causes a stress in the sample, the time dependence of which can be well fitted with a first order exponential decay function as given in Equation 6 (see Section 3.2).

3. Results

3.1. Structure analysis by SEM

The structure of the fibril network of the studied hides changes continuously from the grain towards the corium layer (see Fig. 4A and D). In the grain layer near the surface of the hide the fibrils are packed in relatively small bundles. The average diameter of these bundles is $\approx$2 μm. They are composed of about ten fibrils with a typical diameter of several hundred nanometer. Often, these bundles do not exhibit a cylindrical shape, but show a more plate-like or lamella-like structure. In addition, we observe large regions of loosely tethered fibrils which, in contrast to the crystal-like arrangement of the fibrils in the tightly packed bundles, can be considered as an amorphous phase.

Towards the corium layer the diameters of the bundles grow. At the same time the amorphous regions vanish increasingly and can be only found in the margins and crossing points of fibril bundles. Further below, the structure of the cross section remains fairly constant. Here, the bundles having a diameter of $\approx$100 μm are tightly packed.

The description of the section cut of the hide given above is not specific only to one particular sample, but it can be regularly found regardless of the applied tanning and drying processes. Nevertheless, the direct comparison between Fig. 4A and D shows that the particular way of drying has large influence on the leather structure as a whole. While acetone drying resulted in a sample thickness of 2.4 mm (Fig. 4A), the thickness of the air-dried sample is only 1.0 mm (Fig. 4D), although both samples have been initially prepared from the same material. Furthermore, air-dried leather is much harder than the acetone-dried one. This draws attention to the fiber isolation, which differs considerably depending on the applied drying process. The large influence on both fiber alignment and isolation is caused by the difference of the surface tensions of acetone and water, leading to different capillary forces in the porous leather during its drying.

TABLE I Characterization of the porosity, derived from both density and SEM feature analysis, and of the specific surface analysis of the investigated samples

	Acetone-dried chrome leather	Air-dried chrome leather
Apparent density (g/cm^3)	0.52	0.65
Porosity from density (%)	57	44
Porosity from SEM feature analysis (% area of pores)	24	14
Specific surface (BET) (m^2/g)	16.6	0.52

In fact, definite differences in the fiber alignment depending on the applied method of drying are clearly stated in Fig. 4B/C, and 4E/F which show SEM micrographs of the upper corium layer. After air drying, the fiber bundles are packed much tighter together than after acetone drying as it can be easily seen from the direct comparison between Fig. 4B and E. Moreover, in air-dried samples the fibrils, which are the smallest structure elements of the bundles, tend to loose their structure and to denature partially depending on bundle size (cf. Fig. 4F). The periodicity of parallel aligned fibrils located at the surface of larger bundles can be hardly resolved by SEM, whereas single fibrils and amorphous tethered fibrils conserve both their periodicity and cylindrical shape. Larger fibril bundles are clearly separated by pores with diameters comparable to the bundle size. In acetone-dried leather the pores are much smaller and often filled by amorphous tethered fibrils. Here, the periodicity of all fibrils, even in large bundles, can be resolved clearly (see Fig. 4C).

These observations are supported by porosity and specific surface analysis (see Table I). Acetone-dried chrome-tanned leather shows both a higher porosity and a higher specific surface than air-dried chrome-tanned leather. The difference in porosity yields 20–50%, while the difference in the specific surface is a factor of about 30. Both methods give different results, because the routines used to determine the porosity are not sensitive to nano-scale features, neither the calculation from density measurements nor the estimation from SEM analysis. Or in other words, nanopores in-between the fibers, which are not closed by capillary forces during drying, do not considerably contribute to the volume porosity, however they result in a large inner surface of the material. Thus, the large specific surface of acetone-dried leather has to be attributed to a well developed fiber isolation. On the contrary, the isolation of individual fibers in air-dried leather (Fig. 4E/F) is much less than in acetone-dried leather while bundle separation is more pronounced. In comparison to the large difference between the acetone-dried and the air-dried sample, the variation of the specific surfaces of the different sub-layers of the acetone-dried sample is found to be relatively small. The measurement of the specific surface of the grain layer, the upper corium layer and the lower corium layer yielded 25.6 m^2/g, 18.9 m^2/g and 14.4 m^2/g, respectively.

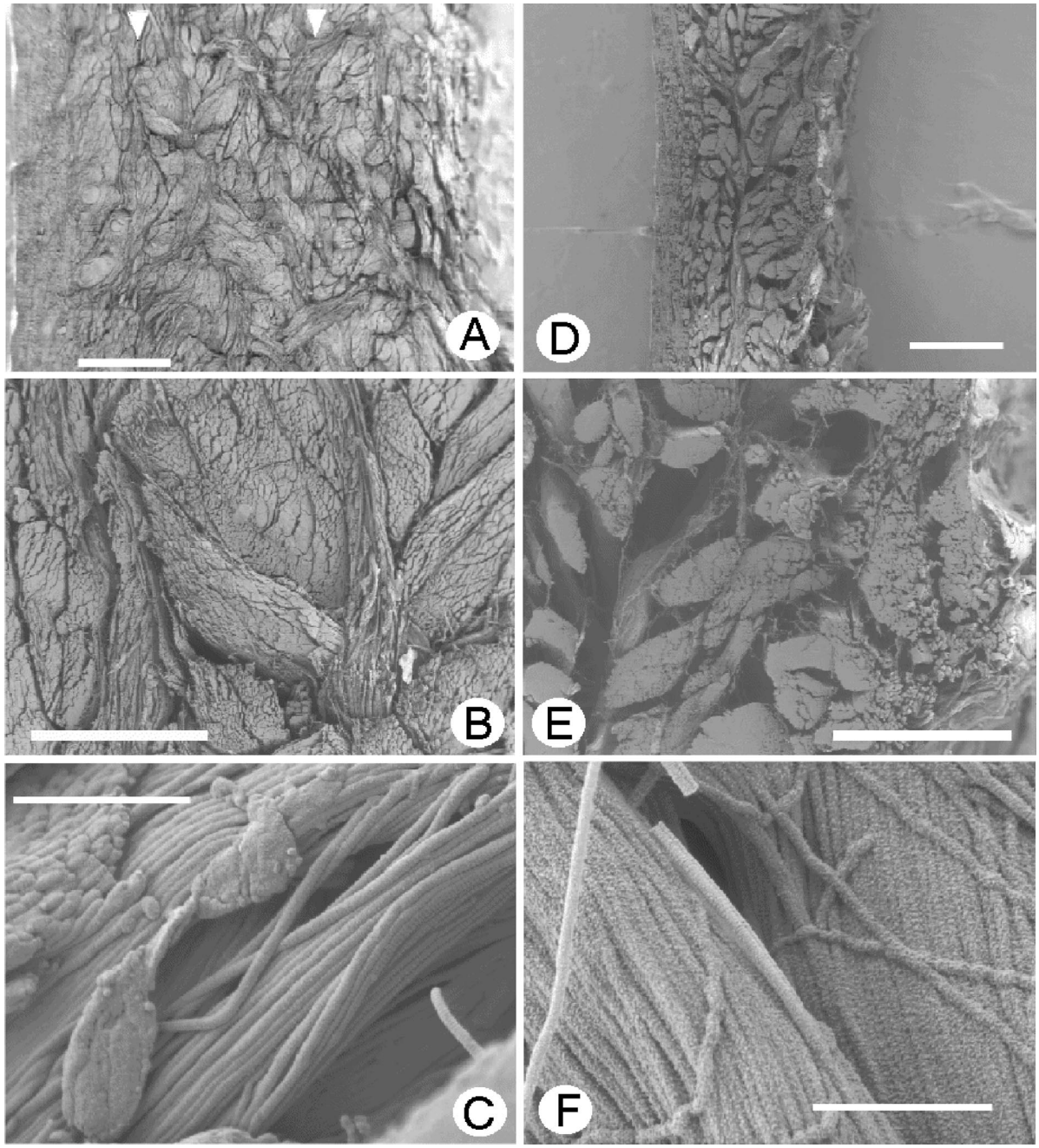

Figure 4 Low voltage scanning electron micrograph of a section cuts of acetone-dried chrome-tanned leather (A–C) and of air-dried chrome-tanned leather (D–E). (A) The white arrows in the top region of the image indicate the border lines between the different layers: (from left to right) grain layer, upper corium layer and lower corium layer. The scale bar denotes 500 μm. (B) Micrograph of the upper corium layer. Scale bar 200 μm. (C) High-resolution micrograph of the upper corium layer. The fibrils exhibit a clear isolation, that is, the fibrils in the bundles are separated from each other. The lateral periodic structure along the fibrils of 67 nm is resolved. Scale bar 2 μm. (D) Section cut of the air-dried leather. Compared to the acetone-dried leather (A), here the sample thickness is considerably smaller. Furthermore, larger pores appear. The scale bar denotes 500 μm. (E) Micrograph of the upper corium layer. Dense bundles with diameters of about 100 μm appear. Scale bar 200 μm. (F) High-resolution SEM micrograph of the upper corium layer. Compared to acetone-dried leather (C), the fibril isolation is rather bad, i.e., they do not separate clearly, but merge into larger bundles. The 67-nm periodicity is hardly resolved. Scale bar 2 μm. All section cuts were prepared with a microtome and coated with Pt prior to imaging.

3.2. Mean stresses in leather under changing relative humidity

3.2.1. Acetone-dried leather

In this Section we compare the stress development in the as-received acetone-dried leather samples to the corresponding contributions of their individual sublayers. For this, first, the as-received leather, and second, samples after splitting into the grain layer, the upper corium layer and the lower corium layer were investigated.

A typical example for the observed stress response of the as-received leather to stepwise humidity changes (standard regime) is shown in Fig. 5. Here, four well-discernible features are important:

First, as expected, the leather contracts when the humidity is lowered and expands in the opposite case. Notwithstanding, in the applied regime the stress amplitude does not develop to its equilibrium value within the half cycle period of 1 h. Thus, exclusively the initial stress development caused by an abrupt humidity change is studied. In additional experiments (not shown) we found that the equilibrium value is only reached after a period of $\approx$5–6 h.

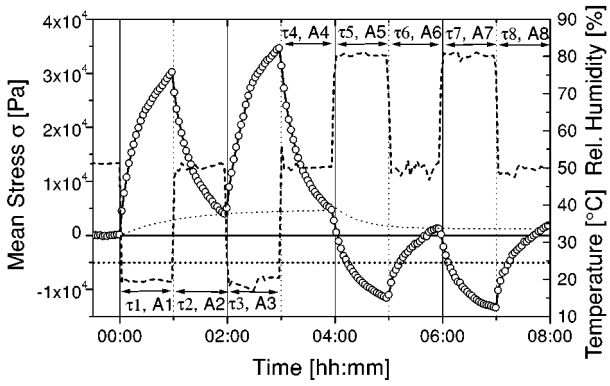

Figure 5 Time dependence of humidity induced stress changes in the as-received acetone-dried leather sample. The stress amplitude (open circles) is plotted together with the relative humidity (dashed line) and temperature (dotted line). Abrupt changes in humidity lead to an exponential stress relaxation (full line: fit of the experimental data). Lowering humidity yields higher stress amplitudes than an increase of humidity.

Second, the reference stress level (corresponding to 50% relative humidity) does not remain constant when the ambient humidity is cycled. Usually an offset is observed the time dependence of which develops exponentially with a typical time constant of about 1–2 h, reaching a constant value after about 3 cycles (not shown). When the sign of humidity change is switched, the sign of the offset will likewise change. As it will be discussed in more detail in Section 3.3, a similar "long-term" relaxation of the 50% reference level was observed for the water sorption of the investigated leather samples.

Third, the time development of the stress can be well fitted with a first order exponential decay function (cf. Equation 6) with a typical time constant of $\tau \simeq 20$ min (after subtracting the above discussed "long-term" contribution to the stress relaxation). That is, the initial stress development can be regarded as an exponential relaxation process. It is worth noting that the relaxation time constant was found to be nearly constant for all humidity cycles independently whether the humidity is increased or lowered.

Fourth, in contrast to the relaxation time, the amplitude of the observed change in stress differs considerably depending on the sign of the humidity alteration. Starting from 50% humidity, the total change in stress is much larger when the relative humidity decreased by 30% in comparison to the case where the humidity increases by the same amount. Thus, the time constant and the amplitude of the humidity induced stress relaxation in leather are independent values which are not directly correlated. This behavior was observed for all measured samples—for the as-received sample as well as for the various sublayers.

The additional investigation of the grain layer, the upper and the lower corium layer revealed that their stress development is very similar to the behavior of the as-received acetone-dried leather in all four items. In particular, we found that the time constants are much the same, whereas the amplitudes of the developed mean stresses decrease with increasing sample thickness. The results are summarized in Fig. 6, where the time constants, τ, and the prefactors, A, derived for different humidity cycles from Equation 6, are plotted versus sample thickness. This plot clearly indicates that both values are rather defined by the thickness of the particularly investigated sample than by the structural differences between grain and corium layer as observed in the SEM investigations.

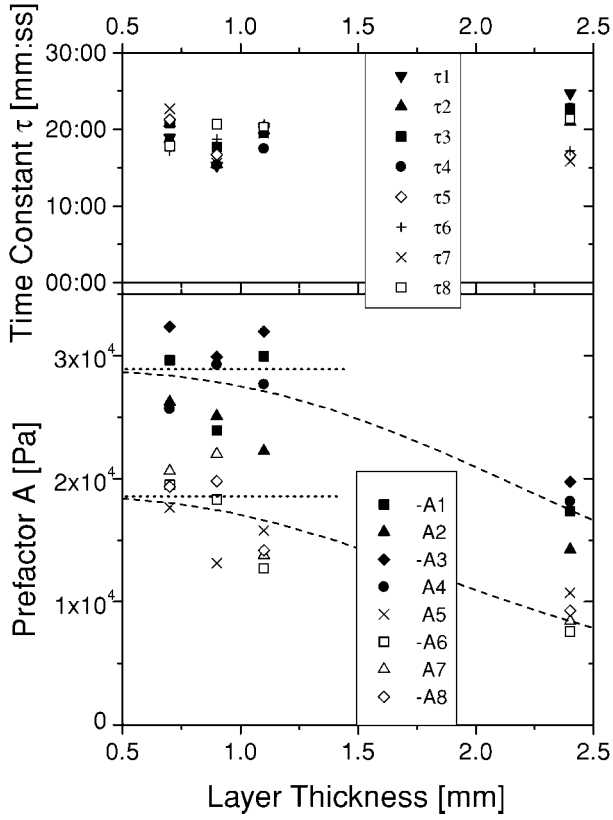

Figure 6 Thickness dependence of the fitting constants for the stress relaxation in acetone-dried leather: the time constants, τ, and the prefactors, A, from the fit of the experimental data of each humidity cycle with Equation 6 are plotted. The amplitudes are clearly separated for different sign of humidity change (open symbols: negative humidity change; filled symbols: positive humidity change). The dashed line denotes the fit of the data point with Equation 5 and the dotted line gives the values in the limit $h \to 0$.

As mentioned above, A decreases with increasing layer thickness. That is, the mean stresses are lower in the entire specimen, (though total forces are of course higher). This behavior is found for both regimes, for positive as well as for negative humidity changes. However, the corresponding stress values are always larger in the latter regime. The fits of the thickness dependence of the A with Equation 5 yield elastic ratios of $e = 3 \times 10^{-3}$ and $e = 5 \times 10^{-3}$ for negative and positive humidity alteration, respectively.

In distinction to that, the calculated time constants, τ, are fairly constant over the whole range of layer thickness. For all thin leather samples, the time constants for positive and negative humidity changes are equal within the errors of the measurement. They do not depend on the sign of humidity change.

3.2.2. Air-dried leather

The response of the mechanical stress in an air-dried leather sample to stepwise changes of humidity (standard regime) is plotted in Fig. 7. The general features

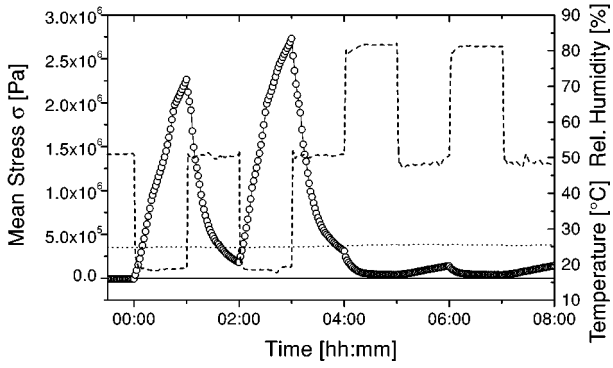

Figure 7 Response of air-dried leather to stepwise humidity changes. The amplitude of the obtained mechanical stress is a factor of 100 higher in comparison to acetone-dried leather (Fig. 5). The symbols are the same as in Fig. 5.

of the time dependence of the stress development is similar to the behavior of the acetone-dried samples, however, the obtained amplitudes are about a factor of 100 larger. In the regime of negative humidity changes mean stress values of $2,5 \times 10^6$ Pa have been obtained. We suppose that this result is a consequence of the pronounced differences in the structure of the both samples after drying.

Despite the large differences in the stress amplitude, the characteristic time constants are found to be nearly the same as in the acetone-dried samples. However, here the time constants clearly depend on the sign of the applied humidity change. Time constants of $\approx$28 min are obtained in the negative humidity-change regime, whereas time constants of $\approx$14 min are calculated for the opposite regime.

3.3. Moisture-sorption characteristic

Parallel to the stress relaxation, the gravimetric mass-sorption kinetics of the samples was investigated. An example is given in Fig. 8, where the relative change in mass of the lower corium layer is plotted versus time. Before starting the experiment the sample was kept at 50% relative humidity over night. Under these conditions the absolute water content in the sample is 18%. The response of the sample is presented for one complete standard humidity regime (cycle numbers 1–8).

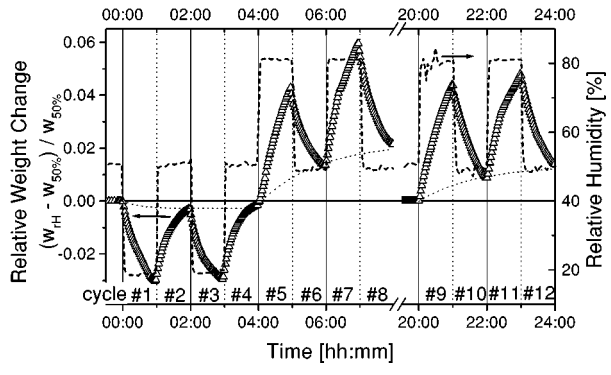

Figure 8 Relative mass analysis of the lower corium layer of acetone-dried leather during switching the relative humidity according to the standard humidity regime (cycles 1–8) and after equilibration for humidity changes between 50% and 80% (cycles 9–12).

In addition, the water-sorption kinetics was repeatedly measured for two complete cycles of humidity change between 50% and 80% (cycle numbers 9–12) after the zero reference level has been reached again within a period of 13 h.

As expected, the weight of the sample decreases, when the humidity is lowered to 20%, and increases, when the humidity is raised to 80%. In the case of equilibrium conditions we would anticipate from the adsorption isotherms [15] a change of the sample mass of about 10% for both signs of humidity alteration. However, the measured mass alterations are found less in all cases. This emphasizes once more that the presented investigations focus especially on the initial period of water exchange far from equilibrium.

It should be noted that the mass reference level (corresponding to 50% relative humidity) does not remain constant when the ambient humidity is cycled. It exhibits initially a similar exponential behavior as the reference level of the stress measurement (cf. Fig. 5. Again, typical time constants of about 1–2 h are found. In order to ascertain whether this "long-term" effect depends on the "pre-history" of the sample treatment, the positive humidity-change cycles were carried out under different conditions. In the beginning, the water sorption (cycle numbers 5–8) was measured directly after finishing two negative humidity-change cycles. Then, with a time lag of 13 h, this measurement was repeated (cycle numbers 9–12). This particular investigation gave two results: First, the observed shift in reference level vanishes again to zero after keeping the sample at 50% humidity for a period of at least 12 h. Second, Fig. 8 shows that the reference level offset does depend on the "pre-history" of the sample. Although the characteristic time constants for both positive humidity-change cycles are found to be similar ($\tau = 107$ min for cycles 5–8, and $\tau = 101$ min for cycles 9–12), the amplitudes of the observed offsets differ. The amplitude is found to be less by a factor of 2 after keeping the sample at 50% humidity for 13 h.

After the correction for the reference level offset, the mathematical analysis of the gravimetric measurements revealed that the mass-sorption kinetics of the leather samples exhibit the same exponential behavior as their stress relaxation. This leads to the conclusion that alterations of moisture content in the material is directly driven by the concentration difference between inside and outside the material:

$$\dot{c} = \frac{1}{\tau} \cdot (\alpha \cdot c_{\mathrm{RH}} - c). \qquad (7)$$

Here, c is the moisture content in the material, c_{RH} is the relative humidity of the ambient air, α is a proportional factor respecting phase transition phenomena like Henry's law, and τ is the characteristic time constant for the process of moisture equilibration. The characteristic time constants of the individual cycles (1–12) together with time constants from another control experiment are given in Fig. 9. It can be seen that in average the time constants for the positive and negative humidity regimes differ. The time constants for negative humidity changes (50%–20%) are equal to the time constants

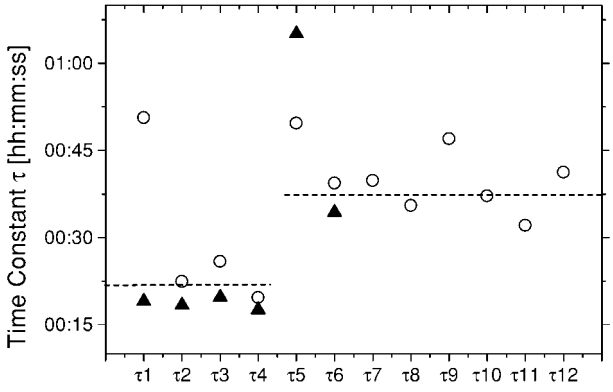

Figure 9 Time constants, evaluated from the relative mass analysis of the lower corium layer. The open circles denote values obtained from the data shown in Fig. 8, and the triangles are derived from a second measurement.

found for the stress development in the same regime. However, to our surprise we found the time constants for the positive humidity change regime (50%–80%) to be larger by a factor of about 2. In addition, Fig. 9 shows that the time constants of respective first cycle of each humidity-change regime (e.g. cycles 1, 5 and 9) tend to deviate from the average time constants. We suppose that this is caused by the large offset of the reference level after the respective first cycle in each humidity-change regime and by the resulting difficulties to deconvolute both time dependent processes properly. The plotted data, however, also manifest that the time constants for the remaining cycles of each humidity-change regime scatter considerably less. Furthermore, the comparison between the time constants for cycles 5–8 with cycles 9–12 shows that the derived time constants do not depend on the "pre-history" of the sample. This also confirms that the applied method of data analysis allows reliable results in experiments which are not carried out under equilibrium conditions.

4. Discussion

A novel method, based on a capacitive transducer technique, has been developed for the measurement of mechanical stresses in planar leather samples. The obtained results for the stress development in acetone-dried and air-dried chrome-tanned leather under changing humidity demonstrate that this method allows the strain-free measurement of stresses with a resolution down to 0.5 Pa. From the maximum measured stresses one can estimate equivalent values for the stress-free deformation by Equation 1, which would be achieved under the ambient conditions described in this work for the hypothetical case of stress-free conditions (i.e. the sample is not fixed to the Si wafer). With a Young's modulus for soft leather of about 10 MPa [3] this would result in a stress-free deformation of about $1 \times 10^{-3} - 3 \times 10^{-3}$. For air-dried leather the stresses are higher, though the Young's modulus should be higher as well. Here, stress-free deformations up to 5×10^{-2} should be reasonable. Thus, it turns out that the loading processes realized in this work range far beyond those of common stress-strain experiments [3].

In addition to the stress development, the water sorption of the leather samples was investigated under the same environmental conditions. Furthermore, the structure of the samples was characterized by SEM and BET. The presented investigations show clearly that the development of mechanical stress in leather is mainly governed by two factors: by the water exchange between the leather sample and its surroundings, and by the internal structure of the fibrillar network. The specific network structure, in turn, is defined by the applied tanning and/or drying process. In particular, the investigated chrome-tanned leathers exhibit well distinct internal structures after application of different drying procedures. The acetone-dried specimens posses a much larger specific surface than the air-dried samples, caused by a more efficient fiber isolation.

Here, we will focus on the discussion of the results obtained for stepwise humidity changes of $\pm 30\%$ starting from a reference level of 50% relative ambient humidity with a cycle period of 2 h. In this "dynamic" regime, both mechanical stress and moisture content are not in equilibrium. However, irrespective of the non-equilibrium conditions, the samples under investigation yielded specific stress responses depending on the applied tanning conditions. Thus, the presented method is well suited for the characterization of particular mechanical properties of leather.

In the presented studies we found that both physical properties of leather, the moisture sorption and the stress development, show a similar time response to abrupt humidity changes. In both cases, an exponential short-time response and a long-term relaxation are observed, which can be understood within the simple model for driven oscillations in RC circuits. The long-term relaxation manifests itself in an exponential time response of the 50% reference level with a characteristic time constant of about 1–2 h. It describes the transient solution of the systems before the system reaches the steady state, where it "oscillates" around the mean value of the driving amplitude. The steady-state solution is characterized by the above mentioned short-time response of the system. Both processes, long-term and short-time relaxation, can be regarded as independent, because differently chosen "pre-histories" of the sample only influenced the long-term relaxation and did not act on the short-time behavior. Thus they can be evaluated separately.

The exponential short-time stress response of acetone-dried samples was studied in great detail for the as-received sample as well as for the individual sublayers. Here, despite the fact that the sublayers exhibit a distinct microscopic structure and a slightly different specific inner surface area, the characteristic time constants were found to be independent of such parameters like the specific type of sublayer, the sample thickness and the sign of humidity change. Within the error of the measurement time constants of about 20 min were derived under varying conditions, pointing out the existence of only one underlying mechanism of stress relaxation. In contrast to the time constant, the stress amplitude after 1 h does depend on ambient parameters. We found that this value is rather determined by the sample thickness than by structural differences of the individual sublayers. The observed thickness dependence can be explained by a simple mathematical

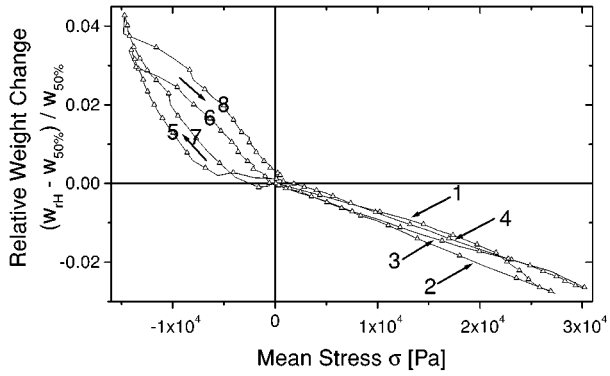

Figure 10 Correlation of the relative weight change and stress development for the same humidity regime.

analysis (cf. Section 2.4) and allows to determine the unknown elastic ratio e of the sample. Furthermore, the stress amplitude depends on the sign of humidity change. Water removal yields higher stress amplitudes than water absorption. This clearly indicates that wet samples allow a local rearrangement of collagen fibrils and fibers whereas a dry sample does not, thus leading to a larger built-up of mechanical stress.

In comparison, the air-dried sample with a well distinct microscopic structure exhibits considerable larger stress amplitudes and distinct time constants for different signs of humidity change. The time constant for the stress development is larger by a factor of two in the negative humidity-change regime than that for the opposite regime. We suppose that both effects are caused by the loss of a nanoscopic fiber separation due to air drying as proved by BET measurements observing a much smaller inner surface area for the air-dried sample.

Now we want to discuss the direct correlation between stress development and driving moisture sorption as illustrated in Fig. 10, where the Figs 5 and 8 are combined by plotting the water content of the sample as a function of mechanical stress for each particular moment of time. This plot shows that the correlation behaves differently at low and at high humidity. Within the errors of the measurement, the low-humidity region exhibits the behavior which is expected for a linear and isotropic material under isothermal condition. According to Equation 1 the stress depends linearly on the water content of the sample. A similar dependence is found in the high-humidity region; however, the main slope of the curve is different in comparison to the low-humidity region, and a pronounced hysteresis is observed. The hysteresis is mainly caused by the fact that time constant for the water sorption (cf. Fig. 9) is larger than that for the stress development. Or in other words, the stress in the sample grows faster than the driving change of water content in the sample! To explain this relatively unexpected result, we have developed the following "two-capillary model", schematically presented in Fig. 11. For simplicity, the model assumes the existence of two types of capillaries in the collagen network with well distinct radii. We will show that in this case the main stress alteration in the sample arises from filling and emptying the capillary system 1 with the smaller diameter, whereas capillary system 2 acts basically as

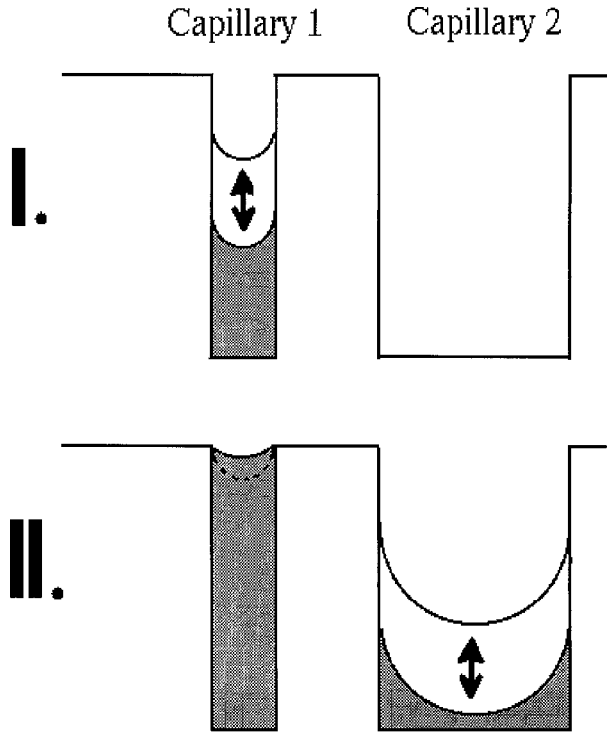

Figure 11 Schematic viewgraph of the "two-capillary model". In the low-humidity regime (regime I) a liquid water phase is only formed in the small capillaries. At high-humidity (regime II) water condenses in both types of capillaries. In addition, the capillary tension in capillary 1 is changed due to the altered vapour pressure (see Equation 8).

a water reservoir without contributing substantially to the stress development. Such system allows to describe the observed differences in the time constants for stress development and water sorption as observed in the positive humidity-change regime.

Filling of the system takes place by capillary condensation, where an undersaturated vapor can coexist with a liquid phase in small pores or capillaries [16]. This phenomenon can be well described by the Kelvin equation [17]

$$\ln S = -\frac{\gamma \cdot v_{\mathrm{m}}}{k_B T} \cdot \kappa_{\mathrm{l}}, \tag{8}$$

where $S = \frac{p}{p_0}$ is the vapor saturation ratio with p is the actual vapor pressure and p_0 is the saturation vapour pressure of the liquid. γ is the surface tension of the liquid, v_{m} is its molecular volume, and κ_{l} is the curvature of the liquid surface. The curvature is, for ideal wetting, given by $\kappa_{\mathrm{l}} = \frac{1}{r}$, where r is the capillary radius. The corresponding capillary tension, exerting forces between the structural elements of the filled capillary, can be calculated by $\sigma_{\mathrm{cap}} = 2\gamma \cdot \kappa_{\mathrm{l}}$.

According to Equation 8, at low humidity only the small capillaries will be filled since the water partial pressure, i.e. the relative humidity, is below the level at which condensation in the larger capillaries can occur (corresponding to regime I in Fig. 11). Thus, the stress in the bulk material is exclusively governed by water in the small capillaries, leading to a direct correlation between moisture content and stress.

When working at high vapour pressure (regime II) both types of capillaries will be involved in the water

sorption and consequently in the stress development, but they act differently. Due to the enhanced vapour pressure, the curvature of the liquid surface of the now completely filled small capillaries will decrease (cf. Equation 8) and, hence, the capillary tension will change. At the same time the systems starts to fill-up the wider pores. Their volume is larger. That means, in the wider pores more water has to be condensed to achieve the same amount of capillary tension change as in the smaller pores leading to an increase of the characteristic time constant for the water sorption in this regime. However, in comparison to regime I the time constant for the stress development remains unchanged since the altered capillary tension in the smaller capillaries dominates the process of stress development. The same behavior is expected when the humidity is lowered again because the model is reversible. That is, the characteristic time constant for water exchange is always longer than the time constant for the stress development in regime II, independently whether the water is adsorbed ore removed. This explains the hysteresis observed in Fig. 10.

The above discussed two-capillary model is also in good agreement with the common water content classification in leather. Relative to dry basis, corresponding to the weight of leather after keeping the sample for 12 h at 110°C, the moisture content of leather is 18% at 50% relative humidity. According to Fig. 10, in our experiment the moisture content was changed between 15% and 25%. Here, the lower value is located in the region of molecularly bound water (7%–25% moisture on dry basis), whereas the upper value corresponds to the border between molecularly bound and capillary-bound water (25%–50% moisture on dry basis). Physical evidence for a separate aqueous phase in leather and other protein structures is also described by Bienkiewicz [18] and Shamblin *et al*. [19], respectively. Furthermore, the result is also supported by the calculations of Komanowsky [20], which show that the capillary diameters, relevant for stress development in the relative humidity range of 50% ± 30%, are between 1 and 10 nm. In a collagen network, cavities/capillaries of this size exist between the collagen molecules, the smallest structural elements of the collagen fibrils.

5. Conclusions

Mechanical stresses in planar leather samples are measured with a high accuracy by using a capacitive transducer technique. The method described allows the observation of the stress development, depending on external parameters such as humidity or temperature, without applying any mechanical strain to the sample. The method turned out to be robust. This makes its wide application in leather industry possible. It yields reproducible results, and it circumvents the limitations of the optical displacement detection of the curvature change of the conjoined leather - silicon wafer system due to induced stresses. The method was applied to stress measurements in acetone-dried and air-dried chrome-tanned leather. The stress is caused by shrinkage and swelling of the collage fiber network due to moisture sorption initiated by changing ambient humidity. The two drying procedures applied to the bovine leather yield collagen fiber networks which are completely different at all investigated length scales. They differ in their macroscopic appearance as well as in their isolation of single fibrils at microscopic level. The obviously softer, acetone-dried leather exhibits a much better fibril isolation than the air-dried leather. Also, much more loosely-packed, tethered fibrils are observed between the tightly-packed bundles of fibrils. Therefore, in acetone-dried leather the fibrils are able to re-arrange their network spatially during shrinking or swelling. As a result the induced mechanical stress is ≈100 times smaller than the corresponding stress in air-dried leather.

Both the stress development as well as the water sorption of the samples after a step-change of humidity can be well described by a first-order exponential decay. However, the correlation between both items behaves differently in the positive and in the negative humidity regime. As expected, the induced stress depends linearly on the moisture concentration of the sample in the low-humidity regime. A similar dependence is found in the high-humidity regime, but with a different main slope of the curve. Furthermore, a pronounced hysteresis is observed, which is caused by the fact that time constant of the water sorption is larger than that of the stress development. This unexpected behavior can be explained on the basis of a simple two-capillary model.

The technique offers various approaches for further investigations on leather such as, e.g., the study of the influence of temperature on stress development or the investigation of the drying process of wet leather.

Acknowledgments

We would like to acknowledge many encouraging and helpful discussions with Tilman Taeger. Financial support by the TFL Ledertechnik GmbH and Co. KG and by the Max-Buchner-Forschungsstiftung (Grant-No: 2054) is kindly acknowledged.

References

1. P. L. KRONICK, *Connect. Tissue Res.* **18** (1988) 95.
2. R. G. MITTON and C. PRICE, *J. Soc. Leather Technol. Chem.* **54** (1970) 44.
3. G. E. ATTENBURROW and D. M. WRIGHT, *J. Amer. Leather Chem. Assoc.* **89** (1994) 391.
4. K. N. KUMAR, J. VONCKEN and C. LIJZENGA, *J. Mater. Sci.* **27** (1992) 472.
5. M. J. CIMA and M. J. CHIU, *J. Amer. Ceram. Soc.* **76** (1993) 2769.
6. J. D. WILCOCK and D. S. CAMPBELL, *Thin Solid Films* **3** (1969) 3.
7. R. W. CLINE, T. J. GREYTAK and D. KLEPPNER, *Phys. Rev. Lett.* **47** (1981) 1195.
8. H. HORNAUER, I. PATRIKOS and K. RÖLL, *J. Vac. Sci. Technol.* **41** (1990) 1302.
9. S. LAMPENSCHERF and W. POMPE, *Z. Metallkd.* **89** (1998) 96.
10. S. BRUNAUER, P. H. EMMET and E. TELLER, *J. Amer. Chem. Soc.* **60** (1938) 309.
11. C. S. JOU, S. T. SACKINGER and R. J. FARRIS, *J. of Coatings Technology* **67**(845) (1995) 71.
12. M. FINOT and S. SURESH, *J. of Mechanics and Physics of Solids* **44** (1996) 683.

13. G. G. STONEY, *Proceedings of the Royal Society of London* **A82** (1909) 172.
14. Y. C. FUNG, "Biomechanics" (Springer Verlag, New York, 1981).
15. K. BOKI and N. KAWASAKI, *J. Colloid Interface Sci.* **164** (1994) 364.
16. S. J. GREGG and K. S. W. SING, "Adsorption, Surface Area and Porosity" (Academic Press, New York, 1982).
17. L. R. FISHER and J. N. ISRAELCHVILI, *J. Colloid Interface Sci.* **80** (1981) 528.
18. K. J. BIENKIEWICZ, *J. Amer. Leather Chem. Assoc.* **85** (1990) 309.
19. S. L. SHAMBLIN, B. C. HANCOCK and G. ZOGRAFI, *European Journal of Pharmaceutics and Biopharmaceutics* **45** (1998) 239.
20. M. KOMANOWSKY, *J. Amer. Leather Chem. Assoc.* **85** (1990) 6.

Received 22 September 1999
and accepted 24 May 2000